



*Supplement of*

**Response of particle number concentrations to the clean air action plan: lessons from the first long-term aerosol measurements in a typical urban valley in western China**

**Suping Zhao et al.**

*Correspondence to:* Suping Zhao (zhaosp@lzb.ac.cn)

The copyright of individual parts of the supplement might differ from the article licence.

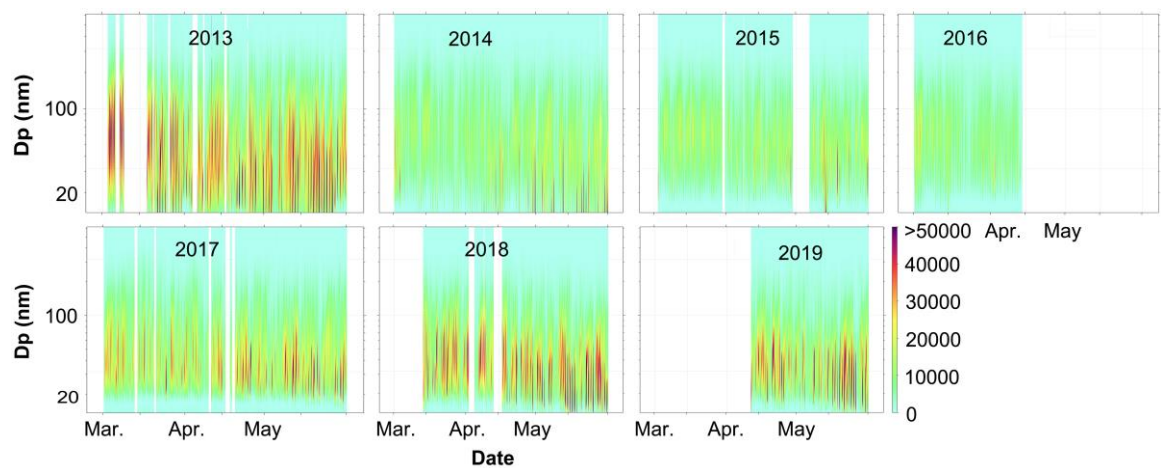


**Figure S1: Evolutions of hourly average particle number size distributions (PNSD) in spring for each year during the campaign. The white gaps in the subplots represent missing data due to failures or routine maintenance of the instruments.**

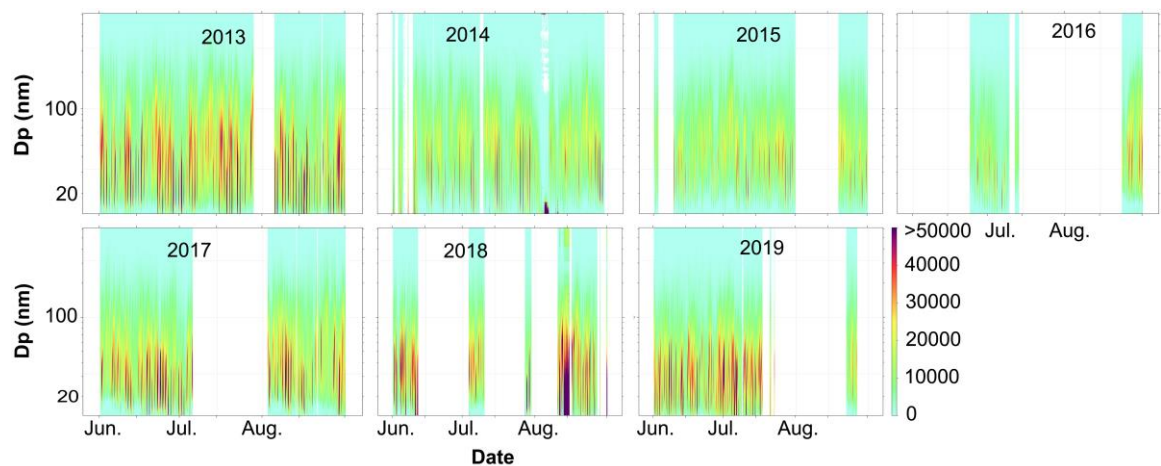


**Figure S2: Evolutions of hourly average particle number size distributions (PNSD) in summer for each year during the campaign. The white gaps in the subplots represent missing data due to failures or routine maintenance of the instruments.**

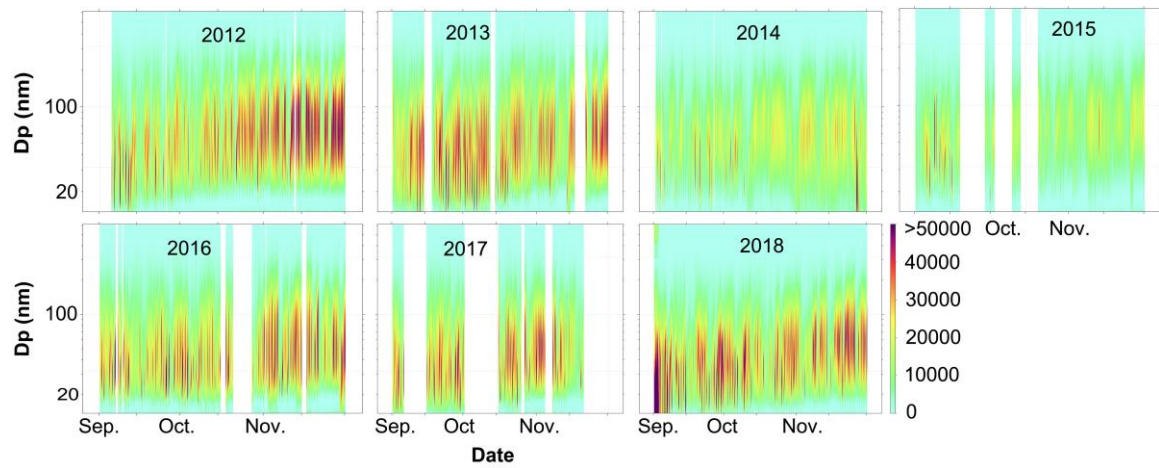


**Figure S3: Evolutions of hourly average particle number size distributions (PNSD) in autumn for each year during the campaign. The white gaps in the subplots represent missing data due to failures or routine maintenance of the instruments.**

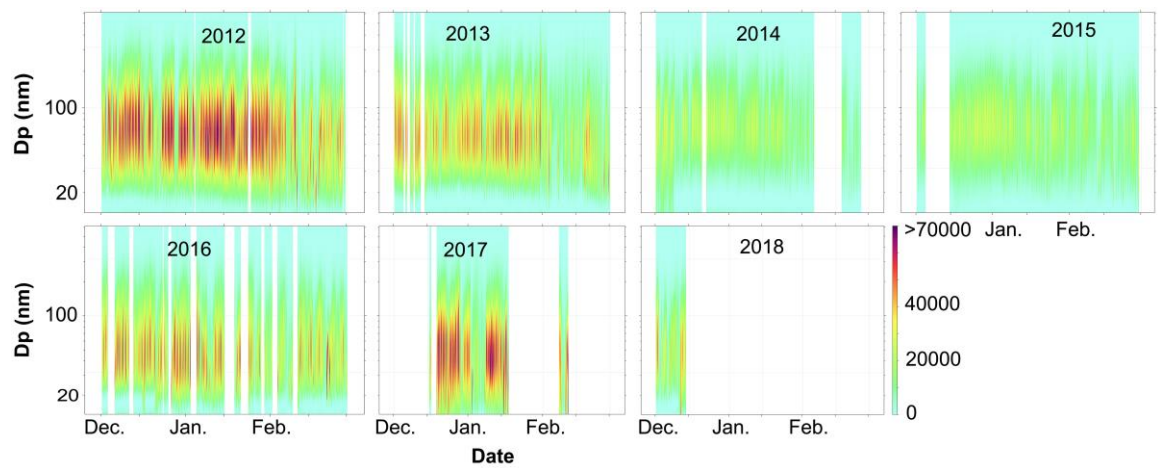


**Figure S4: Evolutions of hourly average particle number size distributions (PNSD) in winter for each year during the campaign. The white gaps in the subplots represent missing data due to failures or routine maintenance of the instruments.**

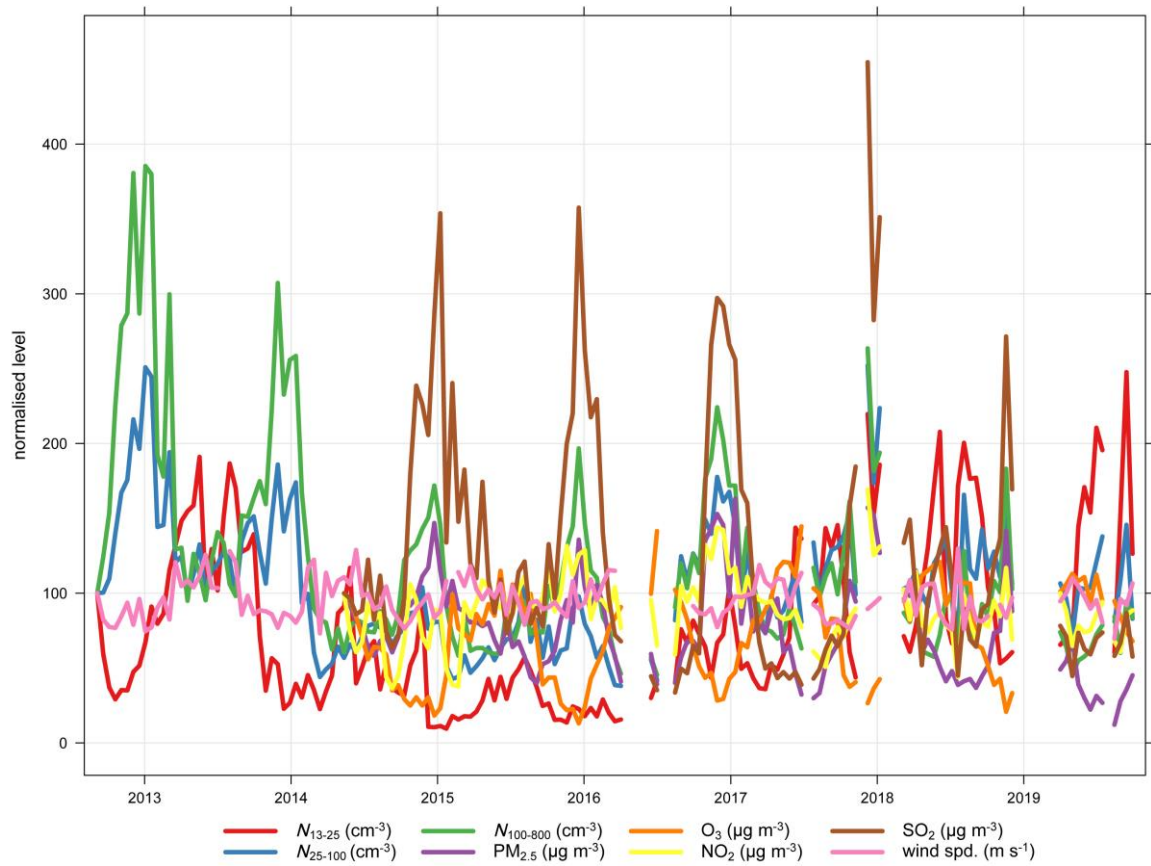


**Figure S5: Normalizing time series of monthly averaged data ( $N_{13-25}$ ,  $N_{25-100}$ ,  $N_{100-800}$ ,  $PM_{2.5}$ ,  $O_3$ ,  $NO_2$ ,  $SO_2$ , wind speed) to fix values to equal 100 at the beginning of September 2012 during the campaign.**

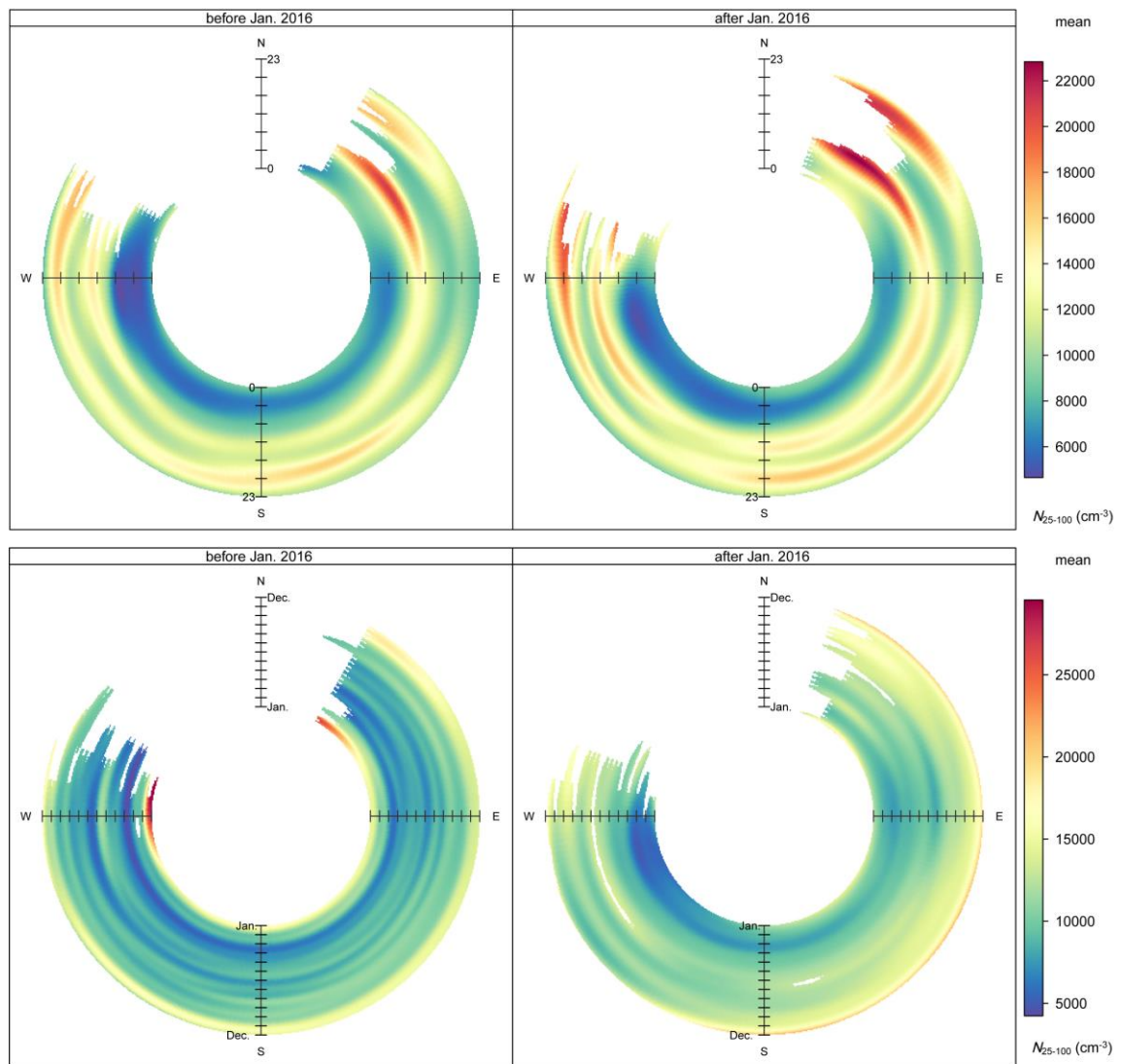


**Figure S6: Mean diurnal (upper panel) and annual (lower panel) variations of particle number in 25-100 size bin ( $N_{25-100}$ ) as wind directions in the two contrasting periods (before vs. after January 2016).**

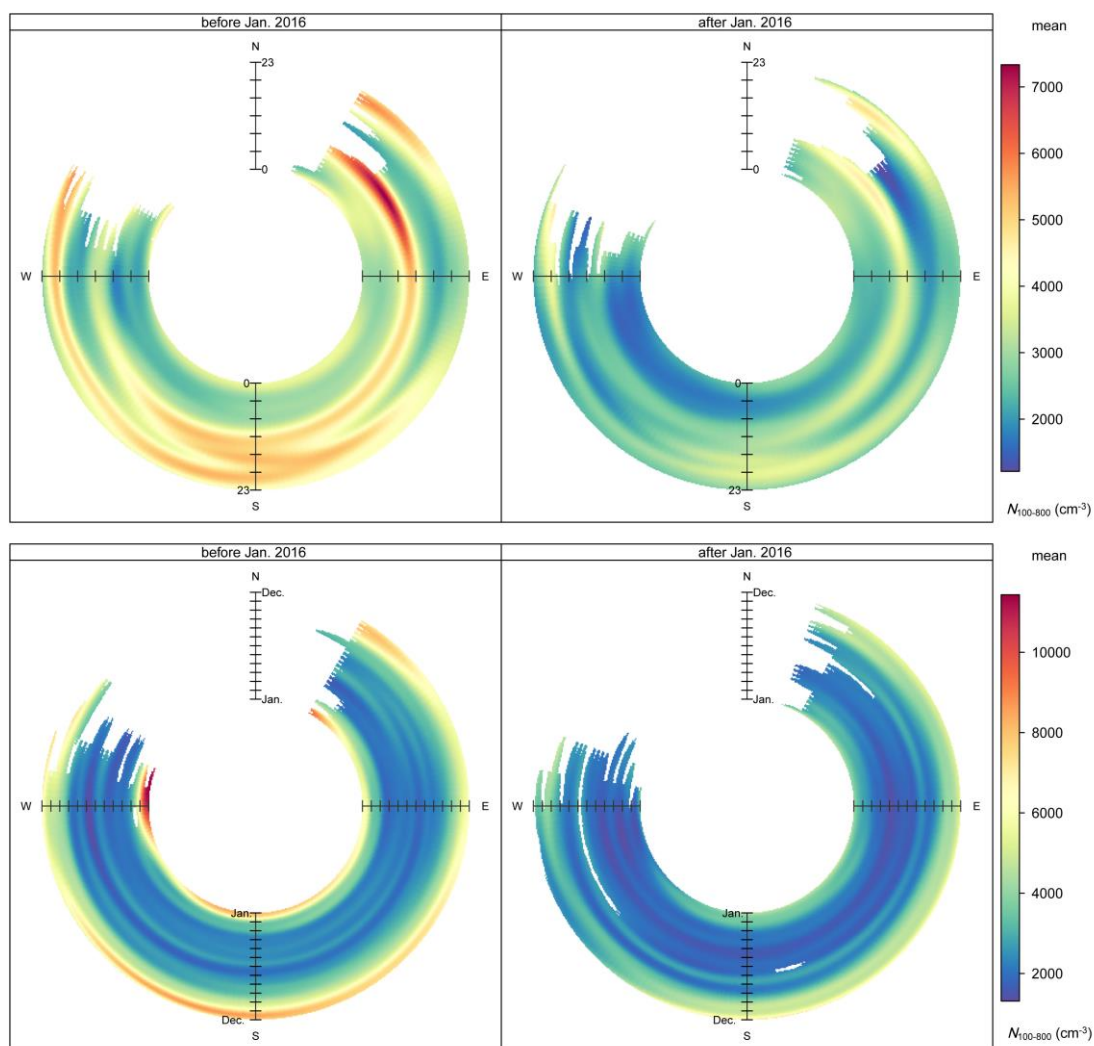


**Figure S7: Mean diurnal (upper panel) and annual (lower panel) variations of particle number in 100-800 size bin ( $N_{100-800}$ ) as wind directions in the two contrasting periods (before vs. after January 2016).**

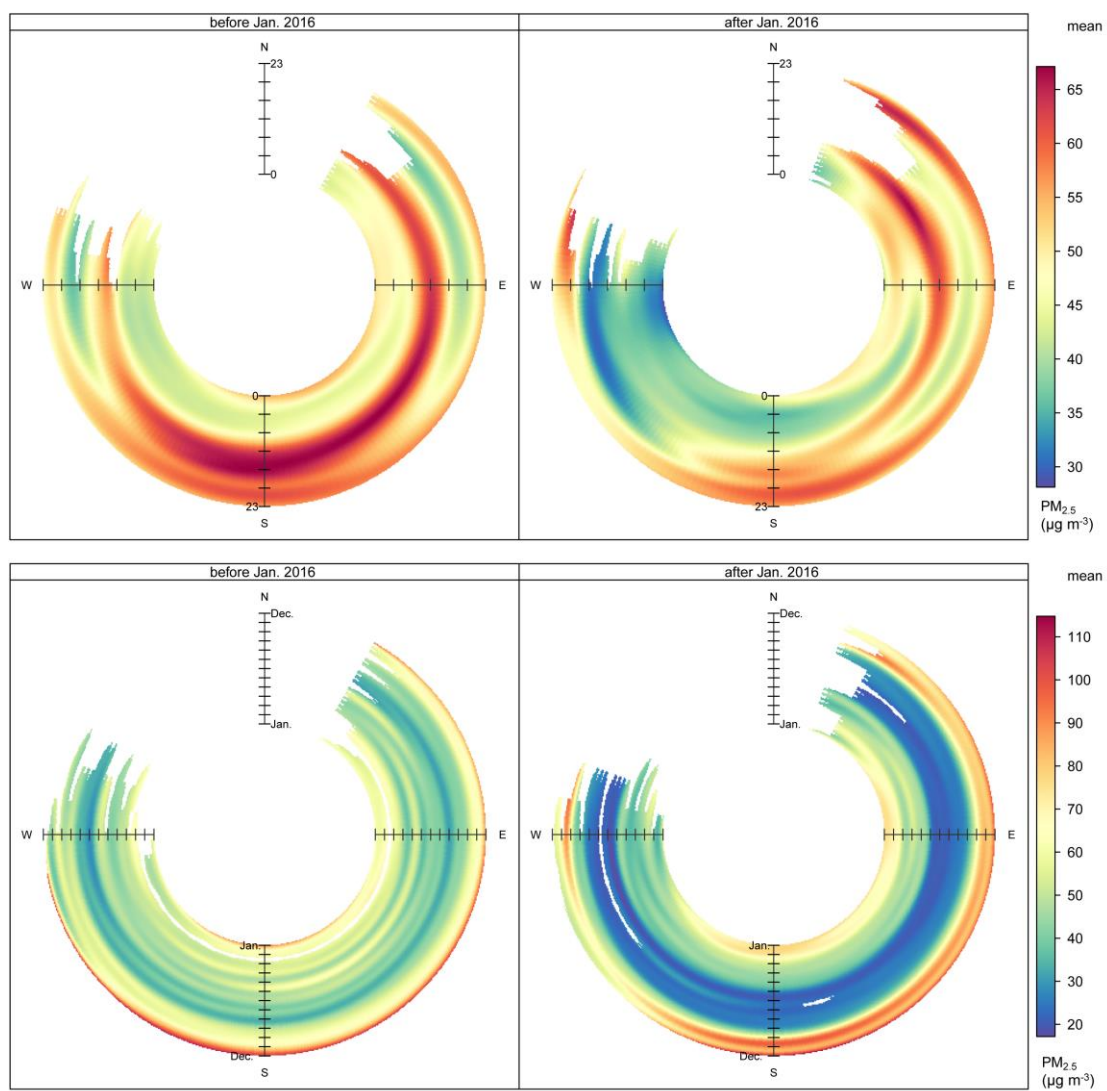


**Figure S8: Mean diurnal (upper panel) and annual (lower panel) variations of  $PM_{2.5}$  as wind directions in the two contrasting periods (before vs. after January 2016).**

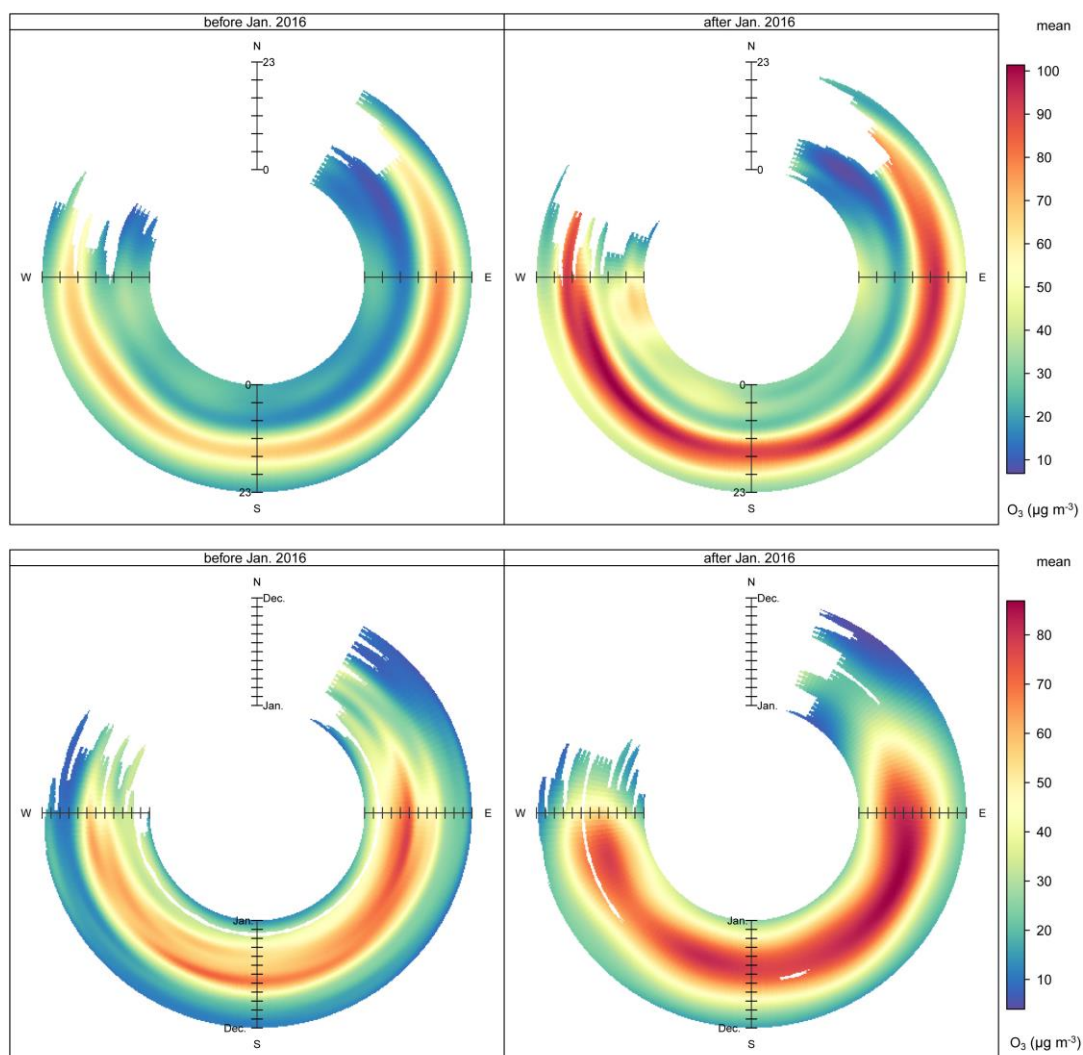


**Figure S9: Mean diurnal (upper panel) and annual (lower panel) variations of O<sub>3</sub> as wind directions in the two contrasting periods (before vs. after January 2016).**

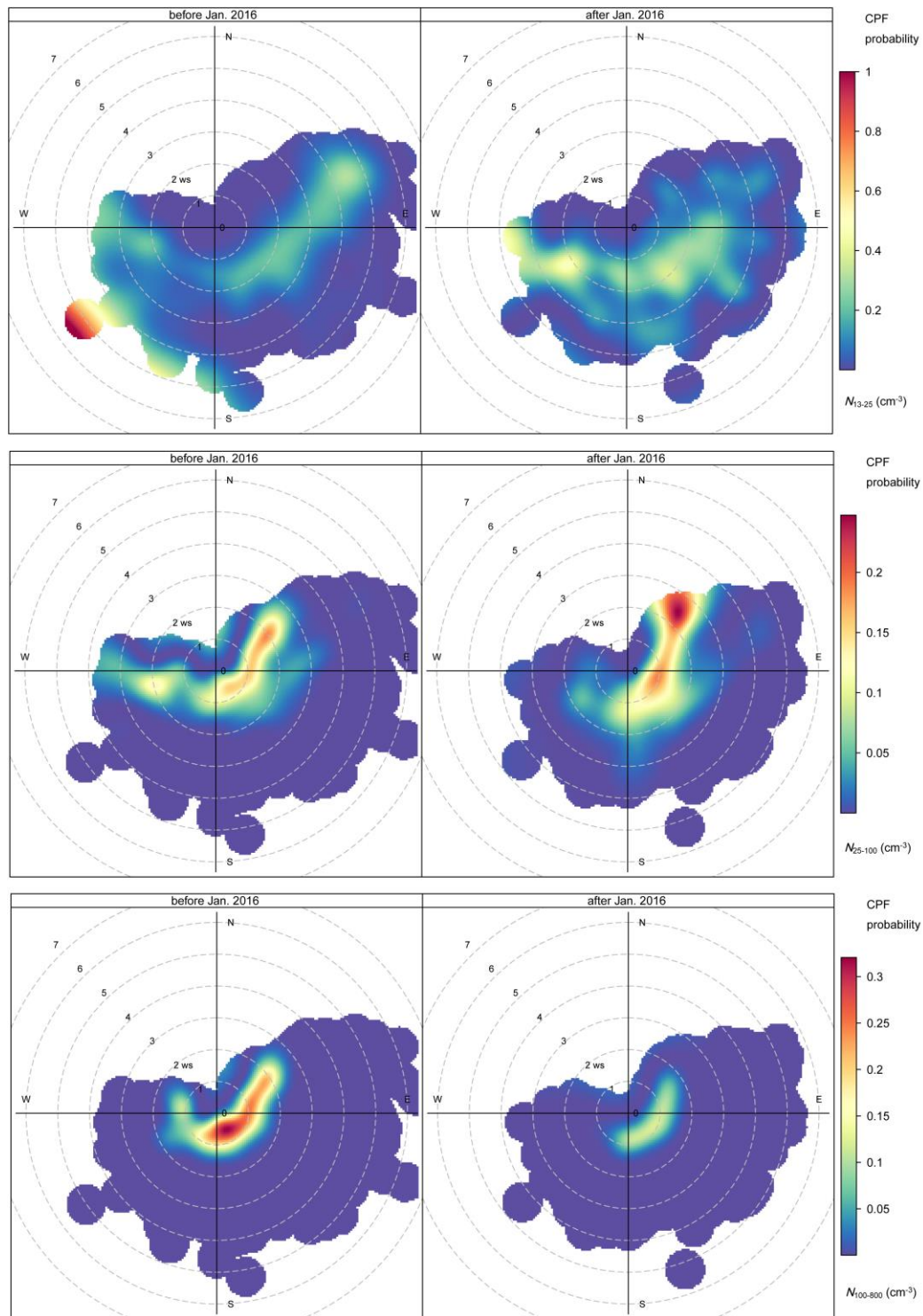


**Figure S10: Polar plot of  $N_{13-25}$  (upper panel),  $N_{25-100}$  (middle panel) and  $N_{100-800}$  (lower panel) based on the CPF function in the two contrasting periods (before vs. after January 2016).**

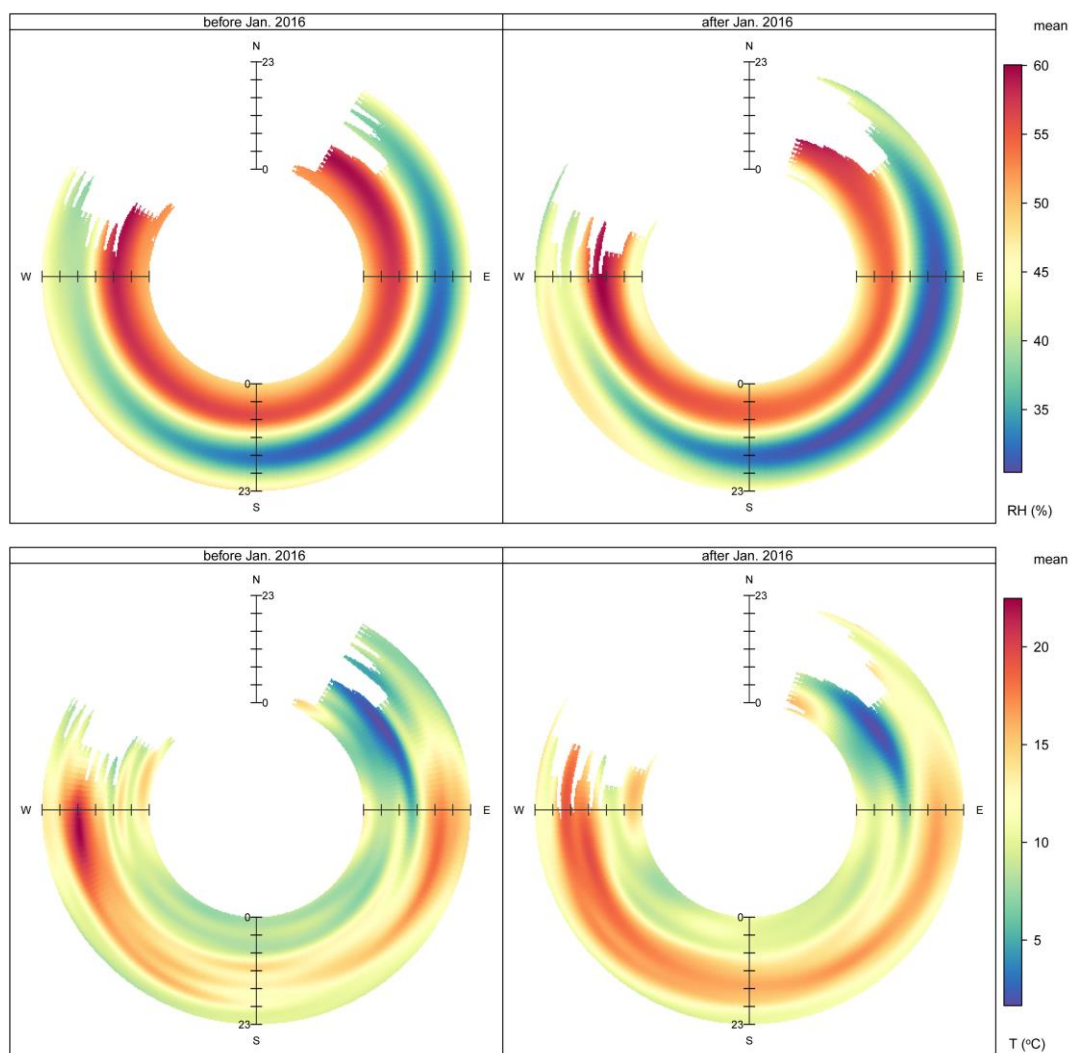


**Figure S11: Mean diurnal variations of relative humidity (RH, upper panel) and temperature (T, lower panel) as wind directions in the two contrasting periods (before vs. after January 2016).**

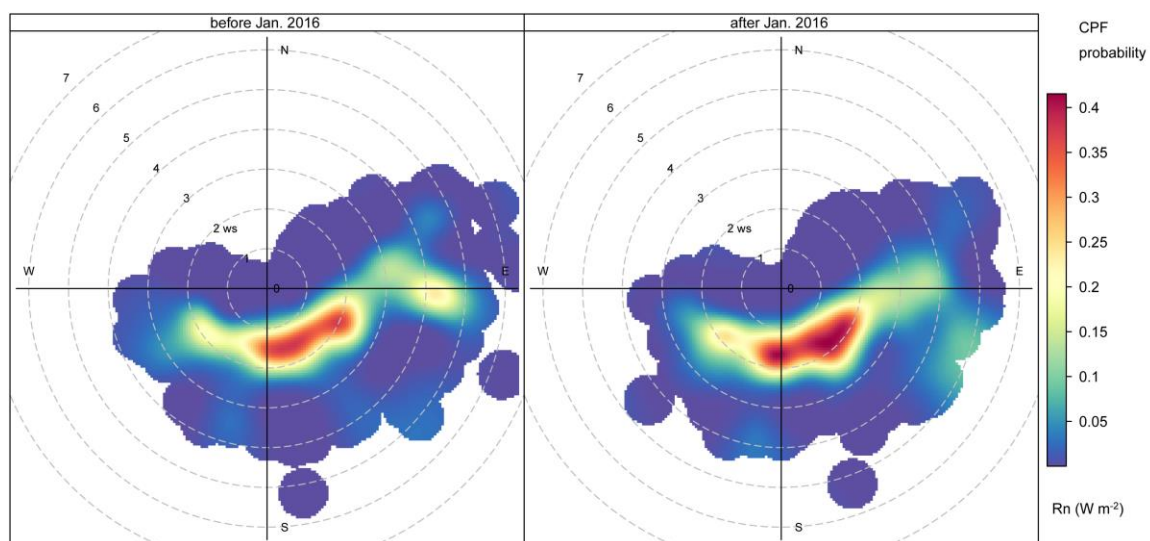


**Figure S12: Polar plot of net radiation (Rn) based on the CPF function in the two contrasting periods (before vs. after January 2016).**

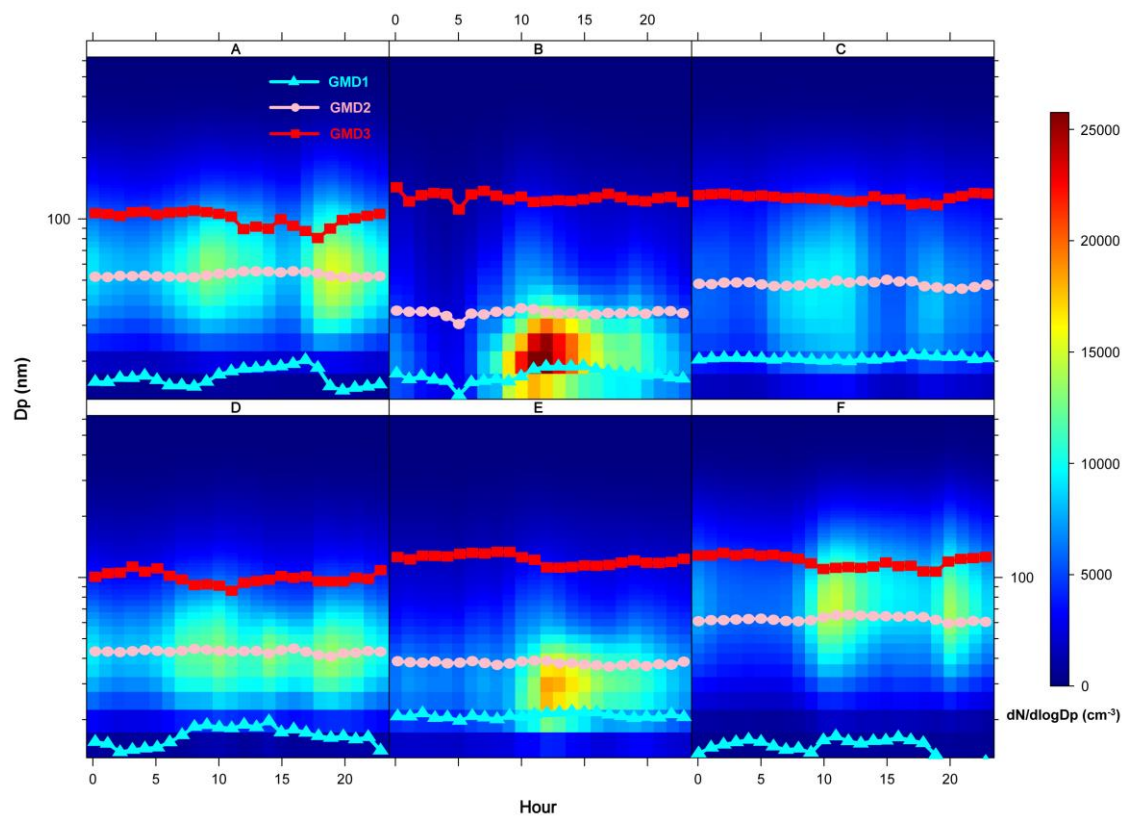


**Figure S13: Averagely diurnal variations of particle number size distributions ( $\text{dN}/\text{dlogD}_p$ ) and geometric median diameter (GMD) of the three modes (GMD1, GMD2 and GMD3 for nucleation, Aitken and accumulation modes, respectively) for Clusters A-F.**

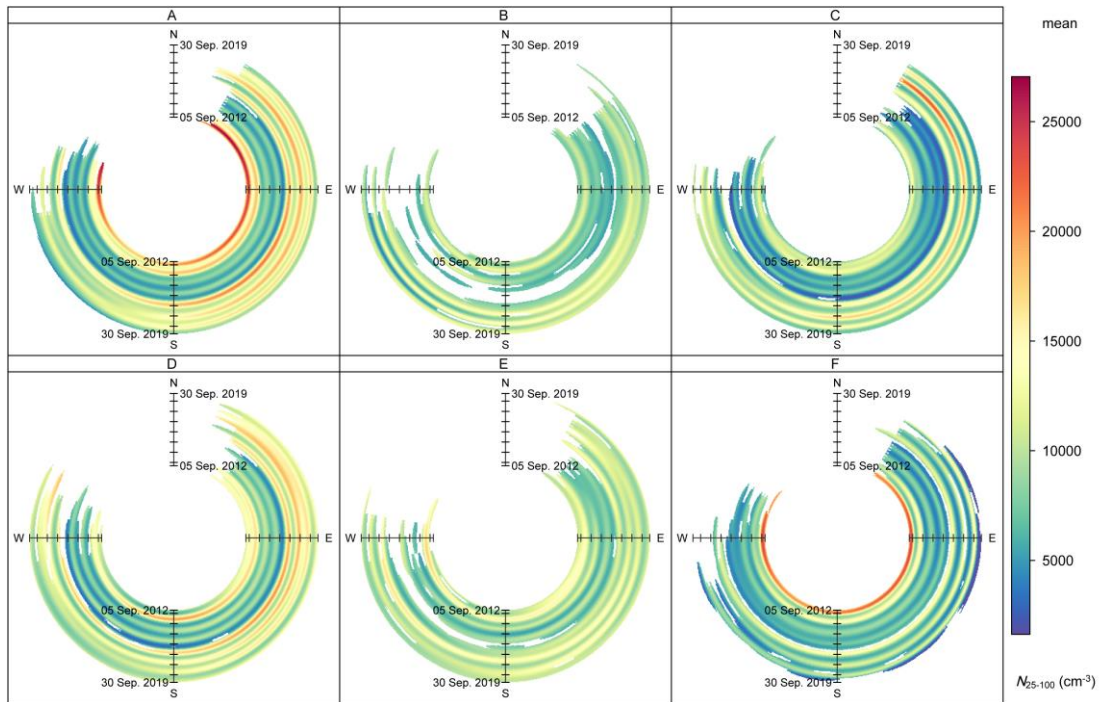


**Figure S14: Trends of daily mean number of particles in Aitken mode ( $N_{25-100}$ ) as wind directions for each cluster during the entire measurement campaign.**

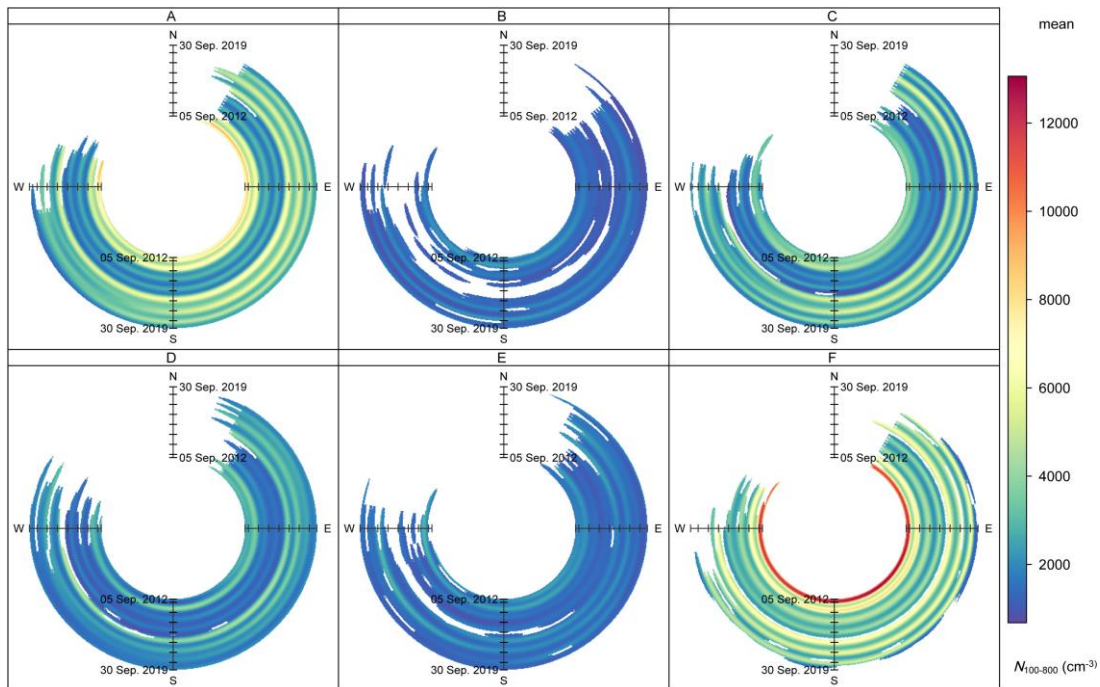


**Figure S15: Trends of daily mean number of particles in accumulation mode ( $N_{100-800}$ ) as wind directions for each cluster during the entire measurement campaign.**

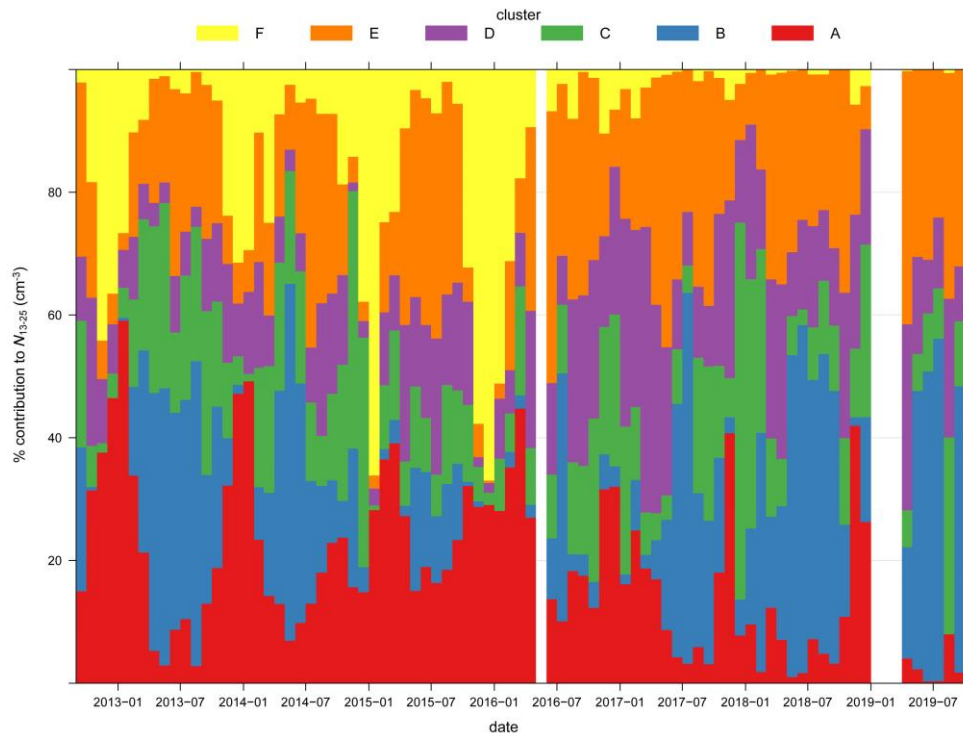


**Figure S16: Variations of contribution of each cluster to monthly averaged  $N_{13-25}$  during the entire measurement campaign. For example, the contribution of Cluster A to  $N_{13-25}$  at a specific month can be calculated by the below equation:  $C_{A, 13-25} = N_{A, 13-25} / \sum N_{13-25} \times 100\%$ . The calculation is similar for the contribution of the other clusters.**

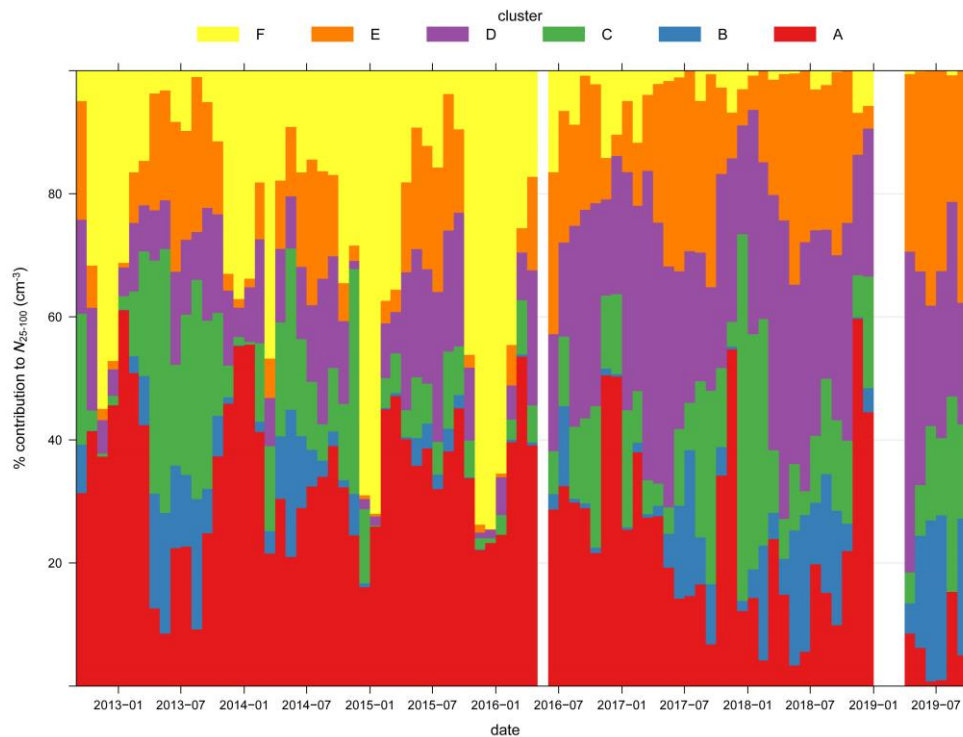


**Figure S17: Variations of contribution of each cluster to monthly averaged  $N_{25-100}$  during the entire measurement campaign. For example, the contribution of Cluster A to  $N_{25-100}$  at a specific month can be calculated by the below equation:  $C_{A, 25-100} = N_{A, 25-100} / \sum N_{25-100} \times 100\%$ . The calculation is similar for the contribution of the other clusters.**

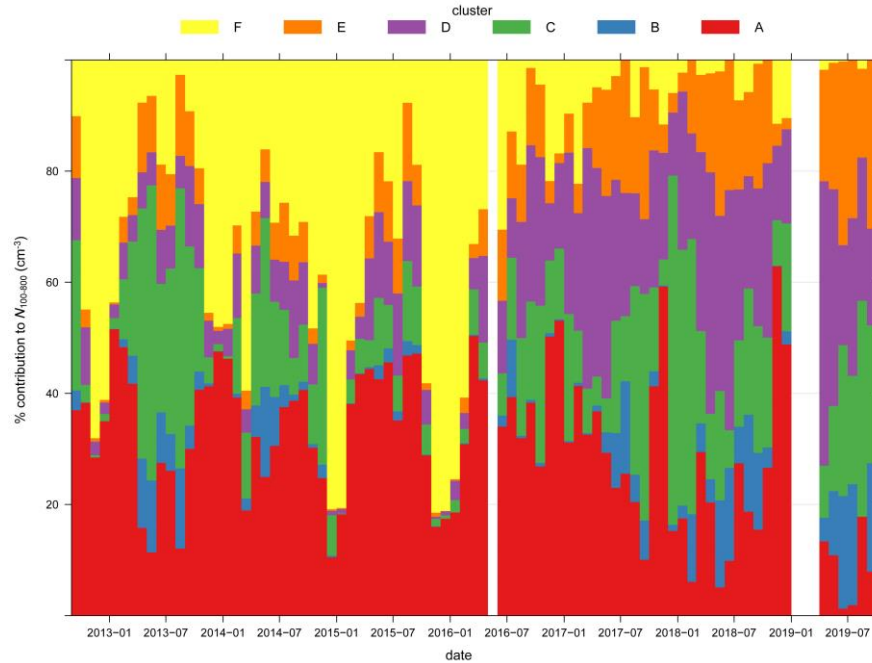


**Figure S18: Variations of contribution of each cluster to monthly averaged  $N_{100-800}$  during the entire measurement campaign. For example, the contribution of Cluster A to  $N_{100-800}$  at a specific month can be calculated by the below equation:  $C_{A, 100-800} = N_{A, 100-800} / \sum N_{100-800} \times 100\%$ . The calculation is similar for the contribution of the other clusters.**

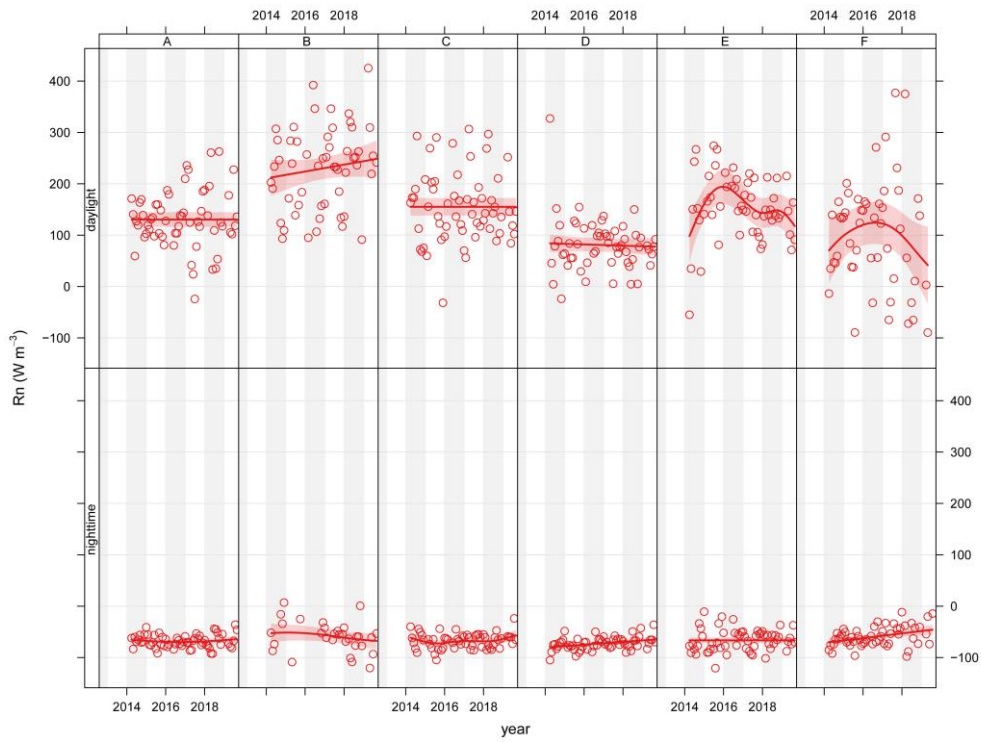


**Figure S19: Inter-annual variations of monthly average daylight and nighttime Rn for each cluster during the campaign. The smooth line is essentially determined using Generalized Additive Model, and the shading shows the estimated 95% confidence intervals.**

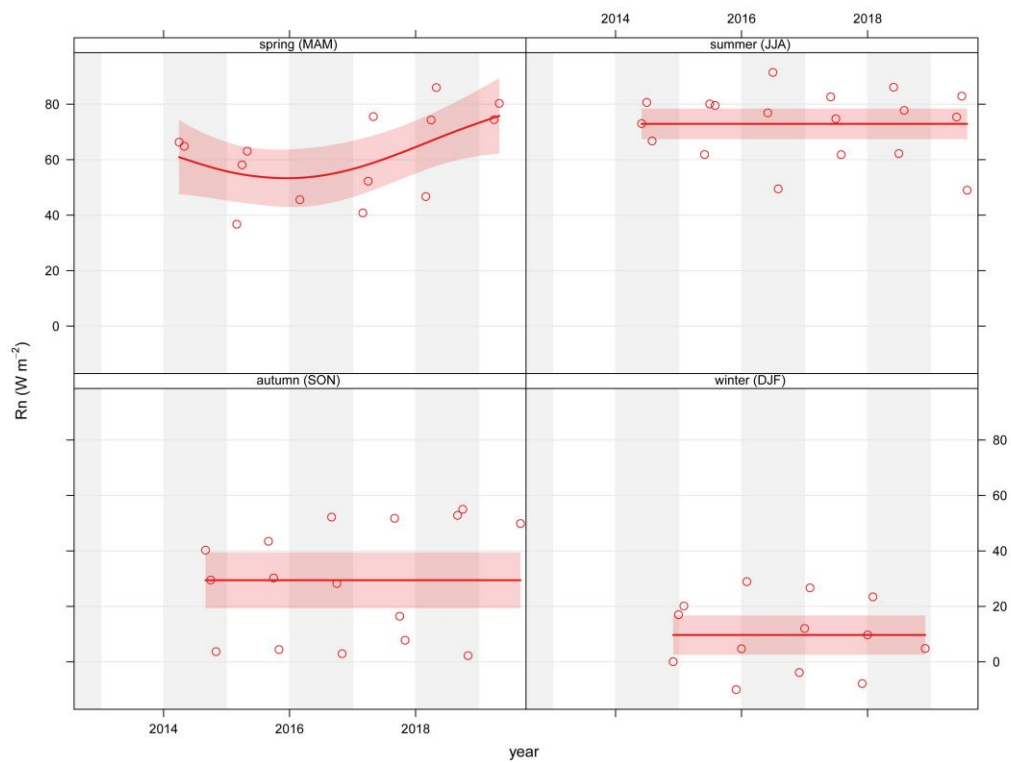


**Figure S20: Inter-annual variations of monthly average Rn in four seasons. The monthly average concentrations are split by year and season. The smooth line is essentially determined using Generalized Additive Model, and the shading shows the estimated 95% confidence intervals.**

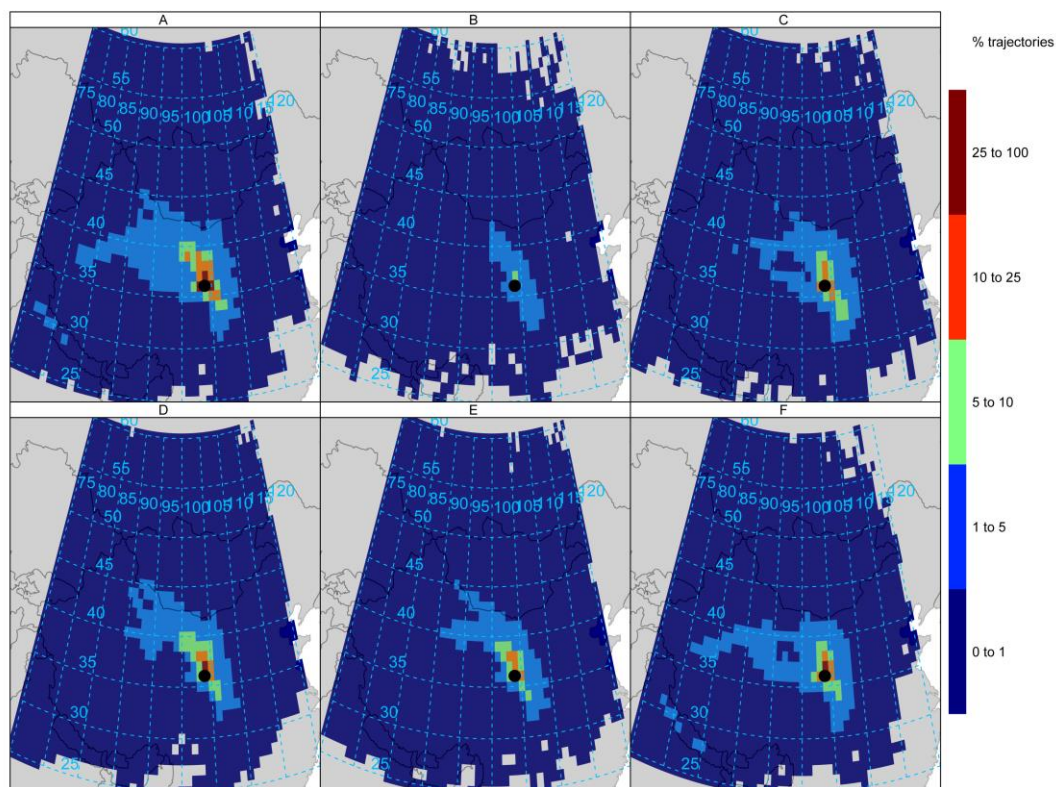


**Figure S21: Gridded back trajectory frequencies for each cluster. The five-day (120 h) trajectories were initialized at 500 m AGL. The black dot shows the geographic location of urban Lanzhou.**